# V.F.2 Performance and Durability of Advanced Automotive Fuel Cell Stacks and Systems

Rajesh K. Ahluwalia (Primary Contact),
Xiaohua Wang, and J-K Peng
Argonne National Laboratory
9700 South Cass Avenue
Argonne, IL 60439
Phone: (630) 252-5979
Email: walia@anl.gov

DOE Manager
Nancy Garland
Phone: (202) 586-5673
Email: Nancy.Garland@ee.doe.gov

Project Start Date: October 1, 2003
Project End Date: Project continuation and direction determined annually by DOE

## Overall Objectives

- Develop a validated model for automotive fuel cell systems and use it to assess the status of the technology
- Conduct studies to improve performance and packaging, to reduce cost, and to identify key research and development issues
- Compare and assess alternative configurations and systems for transportation and stationary applications
- Support DOE and United States Driving Research and Innovation for Vehicle efficiency and Energy (U.S. DRIVE) sustainability automotive fuel cell development efforts

## Fiscal Year (FY) 2015 Objectives

- Establish the uncertainties in system performance due to variability in supporting nano-structured thin film (NSTF) cell polarization data
- Extend system analysis to alternate non-NSTF membrane electrode assemblies (MEAs) with conventional platinum on carbon (Pt/C) and advanced platinum alloy on carbon cathode catalysts
- Incorporate durability considerations in system analysis
- Provide modeling support to Eaton's development of roots air supply system

## Technical Barriers

This project addresses the following technical barriers from the Fuel Cells section of the Fuel Cell Technologies Office Multi-Year Research, Development, and Demonstration Plan:

(A) Durability

(B) Cost

(C) Performance

## Technical Targets

This project is conducting system level analyses to address the following DOE 2020 technical targets for automotive fuel cell power systems operating on direct hydrogen:

- Energy efficiency: 60% at 25% of rated power
- Q/ΔT: 1.45 kW/°C
- Power density: 850 W/L for system, 2,500 W/L for stack
- Specific power: 650 W/kg for system, 2,000 W/kg for stack
- Transient response: 1 s from 10% to 90% of maximum flow
- Start-up time: 30 s from -20°C and 5 s from +20°C ambient temperature
- Precious metal content: 0.125 g/$kW_e$ rated gross power

## Accomplishments

- Showed that the simplified model of calculating stack heat load is quite accurate under most conditions except when a significant fraction of the product water forms liquid, releasing the latent heat of condensation
- Established the uncertainties in system performance due to variability in supporting NSTF cell polarization data: 2–5 \$/$kW_e$ fuel cell system (FCS) cost, 0.02–0.05 g Pt/$kW_e$ platinum content, and 10–15% in power density
- Demonstrated that an alternate first generation (GEN I) catalyst system with conventional high surface area carbon support (d-PtNi/C) has promising performance: 54 \$/$kW_e$ FCS cost and 0.21 g Pt/$kW_e$ Pt content
- Identified the dominant NSTF catalyst degradation mechanism and determined the operating conditions for

20% projected voltage loss at rated power density over 5,000 hours

- Determined the parasitic power requirements of the Roots air supply system: 12.7 $kW_e$ at 100% flow (8 $kW_e$ target) and 295 $W_e$ at idle (200 $W_e$ target)

## INTRODUCTION

While different developers are addressing improvements in individual components and subsystems in automotive fuel cell propulsion systems (i.e., cells, stacks, balance of plant components), we are using modeling and analysis to address issues of thermal and water management, design-point and part load operation, and component, system, and vehicle level efficiencies and fuel economies. Such analyses are essential for effective system integration.

## APPROACH

Two sets of models are being developed. The GCtool (General Computational toolkit) software is a stand-alone code with capabilities for design, off-design, steady state, transient, and constrained optimization analyses of FCS. A companion code, GCtool-ENG, has an alternative set of models with a built in procedure for translation to the MATLAB®/Simulink® platform commonly used in vehicle simulation codes, such as Autonomie.

## RESULTS

In FY 2014, we reported results from a study on an 80 $kW_{net}$ fuel cell system with NSTF ternary catalyst based MEAs, subject to the heat rejection constraint ($Q/\Delta T$ = 1.45 kW/°C) and 40°C ambient temperature [1]. This year, we extended the study to investigate the effect of the stack heat load estimate (Q) on system cost and performance. In our study, Q is the actual stack heat load (AQ) as calculated in the model considering variable $P(O_2)$, $P(H_2)$, $P(H_2O)$, T, and current density along the flow directions. The model includes latent heat released by water condensation (if any) in the stack and the sensible heat transfer to the anode and cathode gases. Besides the cell voltage, AQ should depend on operating conditions such as the operating pressure, temperature, anode/cathode stoichiometry (SR), and rise in coolant temperature ($\Delta T_c$). The heat load in the $Q/\Delta T$ target (simplified Nernst potential [SN]) is written in terms of voltage efficiency ($\eta_V = E/E_N$), defined as the ratio of cell voltage to the Nernst potential ($E_N$):

$$Q = P_s\left(\frac{1}{\eta_V} - 1\right) = P_s\frac{(E_N - E)}{E},$$

where $P_S$ is the stack gross power required for a fuel cell system that generates 80 $kW_e$ net power; the suggested value of $P_S$ is 90 kW. The target also suggests that, for simplicity, $E_N$ be approximated as 1.25 V, independent of the stack operating conditions [1].

Figures 1a and 1b compare the effect of stack heat load estimates (AQ vs. SN) on the cost and performance of the reference system at different operating pressures. Both sets of results, labeled as $Q/\Delta T$ (AQ) and $Q/\Delta T$ (SN), are for optimized $T_c$ and relative humidity (RH) with specified stack inlet pressure (1.5–3 atm), cathode stoichiometry (1.5), rise in coolant temperature (10°C), and Pt loading in anode and cathode. The results show that, under most conditions, Q(SN) is an acceptable approximation to the actual stack heat load, but it grossly underestimates the heat load for conditions under which liquid water forms in the stack and significant amount of latent heat of condensation is released, as at 3-atm stack inlet pressure.

An extensive data base was developed by running more than 130 polarization and electrochemical characterization tests on multiple cells. The reference conditions at 1.5 atm, 2.5 atm, and 3 atm were visited many times during different test series. Figure 1c shows the variability in polarization curves at 2.5-atm reference pressure in two of the eight cells (23102 and 23272); similar variations were also observed at 1.5 atm and 3 atm reference pressures. The inset in Figure 1c identifies the test series in which the data were taken and the order in which the tests were conducted. Figure 1d indicates that the variability in cell voltage ($\Delta V$) is a function of the current density and is higher at higher current density. We may regard $\Delta V$ as a measure of the recoverable losses since the test campaign is not long enough for manifestation of significant irrecoverable losses. In a different study, we confirmed that the voltage losses in Figures 1c and 1d can be recovered by reconditioning the cells by subjecting them to multiple thermal conditioning (TC) cycles. Nevertheless, the variability in cell voltage is representative of the performance variation that may be expected over drive cycles before the onset of permanent degradation mechanisms.

The model discussed in this work is representative (REP) of the average performance in that the kinetic and transport parameters were determined by using the average of all available polarization data. We also developed a model for the best of class (BOC) performance in which we determined the kinetic and transport parameters by using only the best polarization data under different conditions. Figures 1e and 1f compare the FCS cost and performance using the REP and BOC models. Our study shows ~10% improvement in power density (753 $mW/cm^2$), Pt cost (10.8 $/$kW_e$) and stack cost (25.7 $/$kW_e$) if the results for 2.5-atm stack inlet pressure are based on BOC rather than REP polarization data.

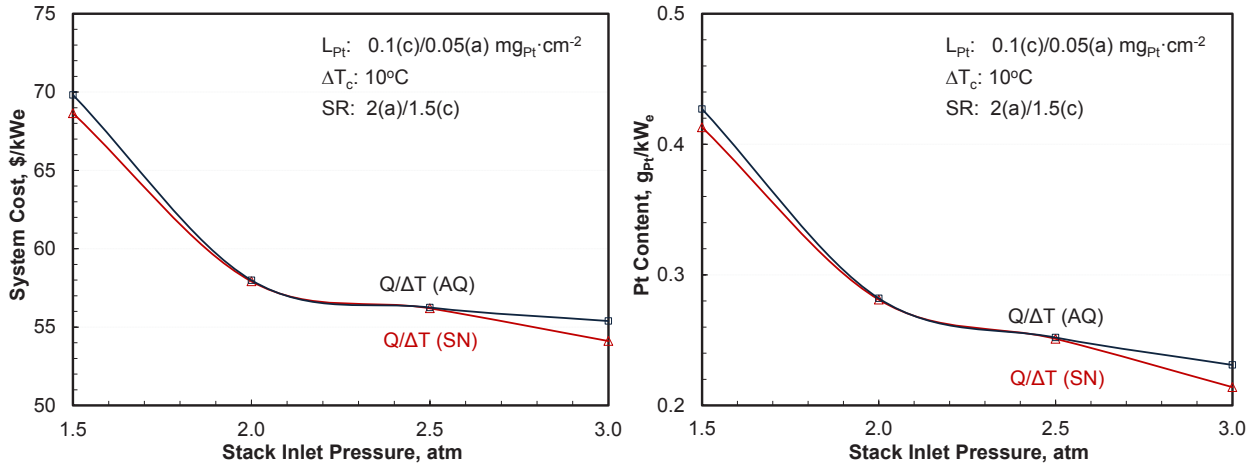


(a) Effect of stack heat load estimate: system cost (b) AQ vs. SN: system performance

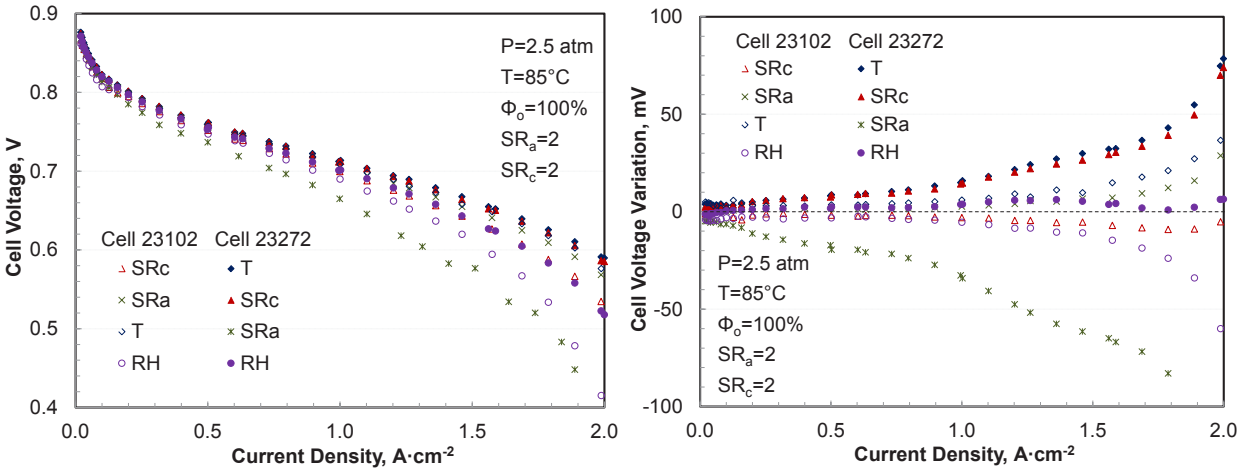


(c) Variability in cell polarization curves (d) Extent of cell voltage variation

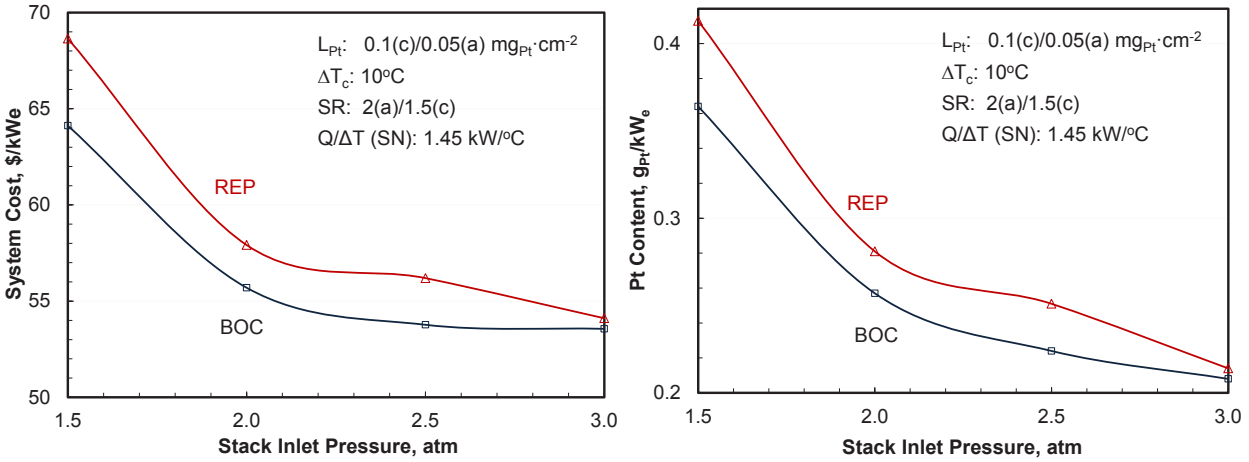


(e) Effect of data variability on system cost (f) Extent of data variability on system performance

**FIGURE 1.** FCS cost and performance studies with ternary NSTF catalyst and Q/ΔT constraint, 0.1 (cathode)/0.05 (anode) mg/cm$^2$ Pt loading, 10°C rise in coolant temperature, 2 (anode)/1.5 (cathode) stoichiometry: (a) effect of stack heat load estimate: system cost; (b) AQ vs. SN: system performance; (c) variability in cell performance; (d): extent of cell voltage variation; (e) effect of data variability on system cost; (f) effect of data variability on system performance

### Alternate Catalyst System

We are collaborating with United Technologies Research Center (UTRC) and Johnson Matthey Fuel Cells (JMFC) to evaluate the performance of an MEA with an advanced cathode catalyst, de-alloyed (d) PtNi/C, relative to the targets of 0.44 A/mg-PGM (platinum group metal) mass activity and 720 μA/cm$^2$-PGM specific activity at 900 $mV_{iR\text{-}free}$, 1,000 mW/cm$^2$ at rated power, and 300 mA/cm$^2$ at 800 mV [2].

We analyzed the hydrogen-oxygen polarization data obtained by UTRC on differential cells (12.5 cm$^2$ active area) with three sets of MEAs supplied by JMFC: d-PtNi/C, high surface area Pt/C, and annealed (a) Pt/C. We developed a step-wise procedure to determine the kinetic parameters of the oxygen reduction reaction (ORR) on d-PtNi/C. Our starting point consisted of using a transmission line model to analyze the hydrogen-air and hydrogen-nitrogen impedance (electrochemical impedance spectroscopy) data for proton conductivity of the membrane ($\sigma_m$) and the ionomer in the cathode electrode ($\sigma_i$). The second step consisted of developing models for distributed ORR in the cathode electrode and distributed hydrogen oxidation reaction in the anode electrode. The final step involved using the known $\sigma_m$ and $\sigma_i$ in these models to determine the ORR kinetic parameters from the measured cell voltage ($E$) in hydrogen-oxygen (negligible oxygen mass transfer losses) at low current densities ($i$). An optimization algorithm was required to determine the Tafel slope since the IR-corrected cell voltage ($E + iR_\Omega$) is not linear with $ln(i + i_x)$, where $i_x$ is the hydrogen crossover current onsistent with the experimental data, the modeled mass activities of d-PtNi/C, 0.533–0.583 A/mg Pt, is higher than the target of 0.44 A/mg PGM. Similarly, the measured and modeled specific activities of d-PtNi/C, 935–1,023 μA/cm$^2$ Pt, are higher than the target of 720 μA/cm$^2$ PGM.

Knowing the ORR kinetic parameters, we analyzed the hydrogen-air polarization data to determine the limiting current density ($i_L$), defined as the current density corresponding to 450 mV mass transfer overpotential ($\eta_m$). We developed empirical correlations for the dependence of $i_L$ on pressure, temperature, $O_2$ partial pressure, relative humidity, and flow rate. We also developed empirical correlations for mass transfer overpotentials by representing $\eta_m$ as a function of the reduced current density ($i/i_L$), pressure, temperature, relative humidity, and air flow rate.

We incorporated the ORR kinetic and proton/oxygen transport aspects of d-PtNi/C electrodes in our large-area cell model. Figure 2a compares the modeled polarization curves for the three catalysts with 0.3 Pt to C and 0.8 ionomer to carbon ratios under conditions required to satisfy the Q/ΔT constraint at 100% exit RH; the modeled curves include additional 10 mV cell-to-stack voltage loss at 1 A/cm$^2$. Compared to Pt/C, d-PtNi/C has 66% higher specific activity (914 μA/cm$^2$ Pt vs. 550 μA/cm$^2$ Pt) but only 17% higher mass activity (0.530 A/mg Pt vs. 0.453 A/mg Pt) because of lower electrochemical surface area (58 m$^2$/g Pt vs. 82 m$^2$/g Pt). Above a critical (crossover) current density, the advantage of higher mass activity of d-PtNi/C is offset by higher mass transfer overpotentials because of smaller surface area and possibly $Ni^{2+}$ contamination. However, in spite of $Ni^{2+}$ leaching out, d-PtNi/C is more durable [3] because its preparation includes an annealing step that grows platinum particles to ~5.1–5.8 nm (~2 nm for Pt/C). Studies have shown that platinum particles smaller than 2 nm are unstable and that the particle diameter needs to be larger than about 4 nm for <30% loss of mass activity after 30,000 potential cycles [4,5].

We analyzed the cost and performance of fuel cell systems with Pt/C, a-Pt/C, and d-PtNi/C cathode catalysts, 1.45 kW/°C Q/ΔT heat rejection constraint, and other assumptions as in Figure 1 for ternary NSTF catalyst. Figure 2b shows that GEN I d-PtNi/C has slight cost ($/kW$_e$) and performance (g Pt/kW$_e$) advantages over Pt/C, especially at low pressures and temperatures. However, as noted above, the high surface area Pt/C is unstable under cyclic potentials, so it may be more appropriate to compare d-PtNi/C with a-Pt/C since the two catalysts have similar Pt particle diameters and should have similar stability. Our model indicates that d-PtNi/C can have 20–30% higher power density than a-Pt/C. Figure 2c shows the relationship between stack inlet pressure and the optimum stack temperature (i.e., coolant exit temperature) for d-PtNi/C. We find that under optimum conditions, d-PtNi/C runs drier at 1.5 atm (88% RH at cathode inlet, 82% at cathode outlet) than at 2.5 atm (82% RH at cathode inlet, 103% at cathode outlet).

### Durability of MEAs with NSTF Catalysts

We collaborated with 3M to develop a test protocol for determining the stability of the baseline ternary NSTF catalyst under potentiostatic conditions. The protocol consists of repeatedly degrading the cell for 10 h at constant potential with periodic fluoride collection and partial reconditioning with one TC cycle. Every 20 h of degradation, polarization curves are taken in hydrogen/air. Every 40–80 hours of degradation, the cell is reconditioned more fully with three TC cycles and data are obtained to measure the cathode ORR activity, cathode electrochemical surface area, hydrogen crossover, shorting resistance, and cell polarization in hydrogen/air.

We received data for three tests run using the above protocol with potentiostatic holds at 0.9 V, 0.6 V, and 0.3 V. The tests were run on 50-cm$^2$ cells with quad serpentine flow fields and ternary catalysts with 0.05 mg/cm$^2$ Pt loading on anode and 0.15 mg/cm$^2$ Pt loading on cathode. The cells used 3M, 825 equivalent weight, membrane that was 20 μm thick. The membrane was chemically stabilized with an antioxidant additive but was not mechanically supported. Even without

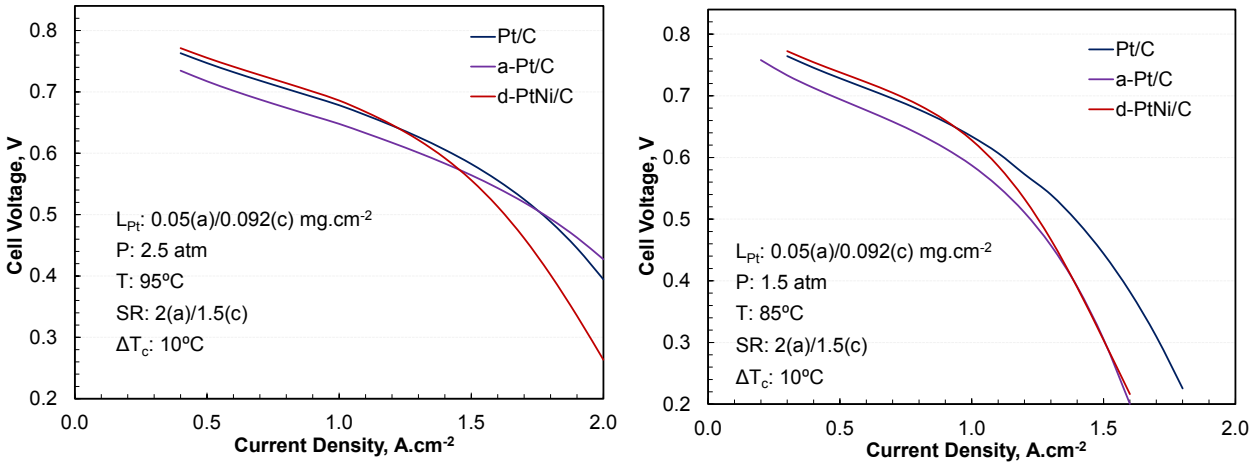


(a) Modeled polarization curves at 2.5 atm (1.5 atm), 95ºC (85ºC), and 100%RH

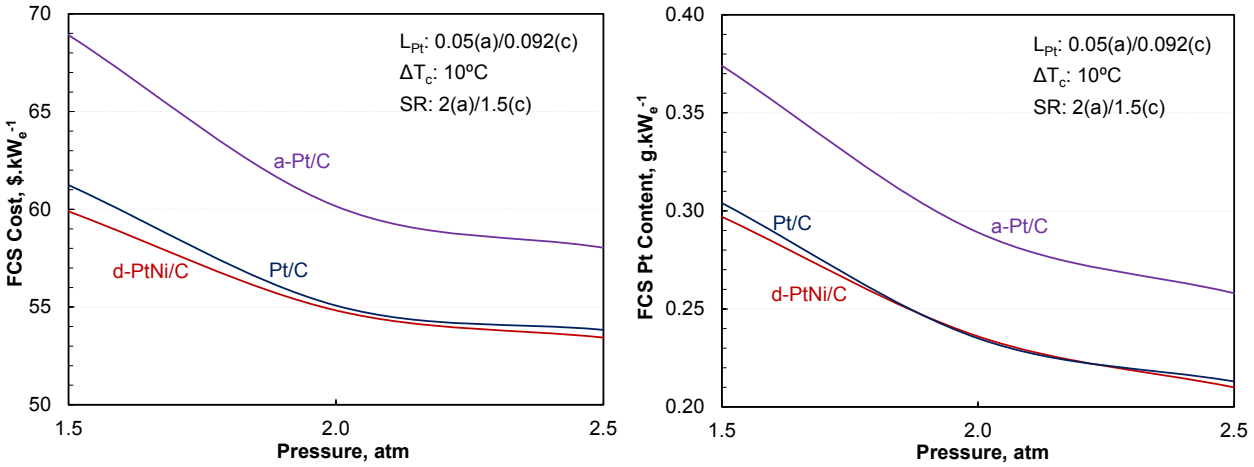


(b) Cost/performance of the three catalyst systems with Q/ΔT constraint (variable P, optimum $T_c$ and RH)

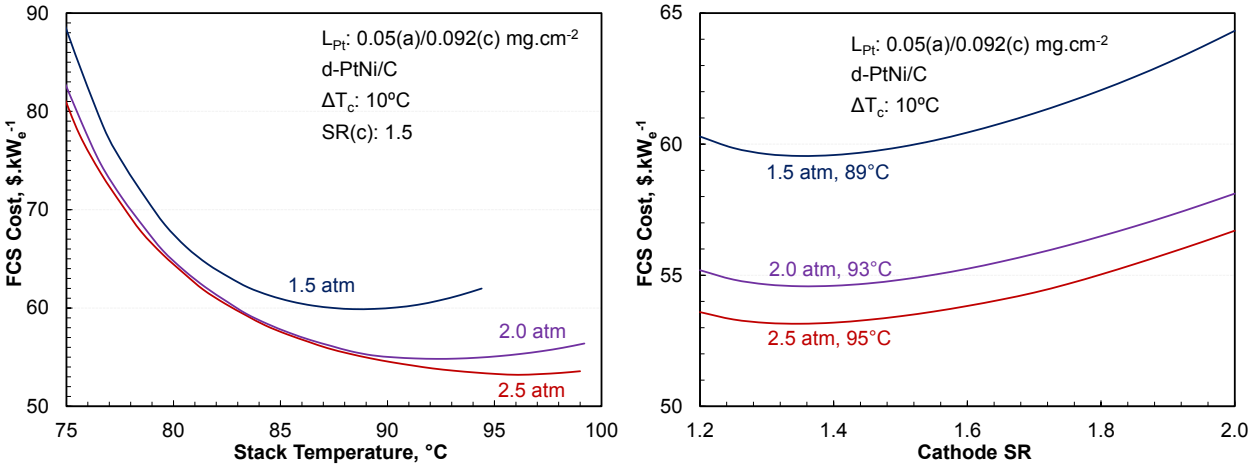


(c) Cost and performance of d-PtNi/C system with Q/ΔT constraint (variable P and $T_c$, optimized RH)

**FIGURE 2.** FCS cost and performance studies with dispersed catalysts and Q/ΔT constraint, 0.1 (cathode)/0.05 (anode) mg/cm$^2$ Pt loading, 10°C rise in coolant temperature, 2 (cathode)/1.5 (anode) stoichiometry: (a) modeled polarization curves at 2.5 atm (1.5 atm), 95°C (85°C), and 100% RH; (b) cost/performance of the three catalyst systems with Q/ΔT constraint (variable P, optimum T and RH); (c) cost and performance of d-PtNi/C system with Q/ΔT constraint (variable P and $T_c$, optimized RH)

mechanical reinforcement, the chemically stabilized membrane remained healthy in that there was no appreciable change in hydrogen crossover or any systematic change in electronic shorting resistance.

The data show systematic degradation in current density during hold at constant potentials. There is a partial recovery of current density after one TC cycle every 10 h; the recovery is more complete with three TC cycles that were imposed nominally every 60 h. Even with three TC cycles, there are irrecoverable losses suggesting permanent degradation. There are also significant differences between hydrogen/air performance after one TC and three TC cycles. The polarization data show incomplete recovery from reversible losses with one TC cycle. With either recovery method, voltage losses are considerably faster at lower hold potentials and are much higher at higher current densities.

The measured loss in cathode surface area (surface enhancement factor or roughness) is nearly independent of the hold potential (see Figure 3a) and may be associated with the dissolution of whiskerettes and the resulting decrease in surface roughness. The data indicate that the ORR absolute and specific activity losses are higher at 0.3 V than at 0.6 V or 0.9 V.

Figure 3b presents the fluoride release rates (FER) measured by ion chromatography of the collected water samples. The measured FERs are an order-of-magnitude smaller than for dispersed Pt/C catalysts with chemically stabilized and mechanically reinforced membranes. Both cathode and anode FERs are higher at lower cell voltages, consistent with the observed dependence of hydrogen peroxide production on potential in rotating ring disk electrode tests.

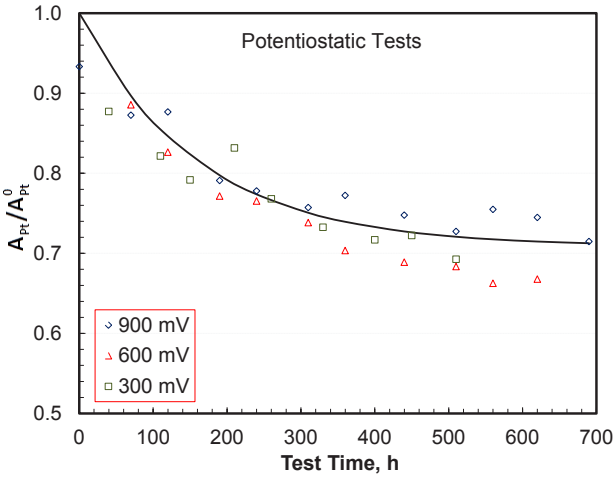


(a) ECSA loss

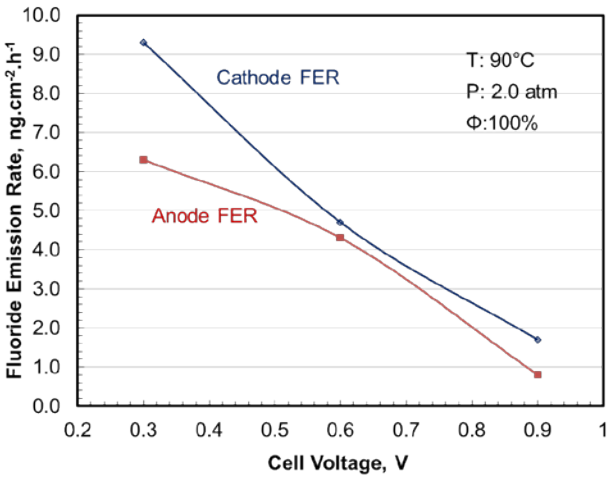


(b) Fluoride emission rate

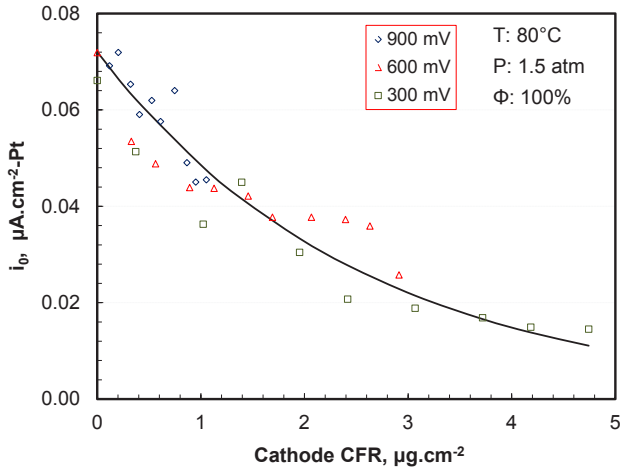


(c) Modeled loss in ORR exchange current density

**FIGURE 3.** Stability of NSTF catalyst based MEA under potentiostatic conditions: (a) electrochemically active surface area (ECSA) loss; (b) fluoride emission rate; (c) modeled loss in ORR exchange current density

We determined the kinetic parameters from the measured cell voltages at low current densities. We calculated small changes in Tafel slope with ageing at potentiostatic hold. We noted that the increase in ORR overpotential ($\eta_c$) is more than the expected increase in $\eta_c$ due to reduction in surface roughness, suggesting that an additional mechanism exists that accounts for the degradation in specific ORR activity.

We developed a correlation for the increase in ORR overpotential with potentiostatic ageing. Figure 3c presents our correlation of the exchange current density (mA cm$^{-2}$ Pt) assuming that the specific ORR activity is only a function of the cumulative fluoride release (CRF) at cathode. Figure 4a shows a 65 mV irreversible increase in activation overpotential ($\eta_c$) during the course of the three tests.

We determined the mass transfer overpotentials ($\eta_m$) from the measured cell voltages and the derived ORR kinetic parameters. The data indicate significant increase in $\eta_m$ with potentiostatic ageing and larger increase in $\eta_m$ at lower hold potentials. We developed a correlation for the limiting current density ($i_L$), defined for convenience as the reference current density at which the mass transfer overpotential ($\eta_m$) equals 200 mV. Figure 4b shows that $i_L$ decreases as more fluoride is released at cathode, probably because of catalyst contamination (not yet characterized).

We also developed a correlation for the mass transfer overpotential ($\eta_m$) assuming that it is only a function of $i/i_L$ and cathode CFR, see Figure 4c. Implicitly, $\eta_m$ is also a function of the hold potential through its dependence on $i_L$. Figure 4d indicates that $\eta_m$ is primarily a function of CFR and current density for 300 mV and 600 mV hold potentials.

In summary, we have confirmed that long potentiostatic hold is a major degradation mechanism for the NSTF catalyst and that the irreversible performance losses are higher at

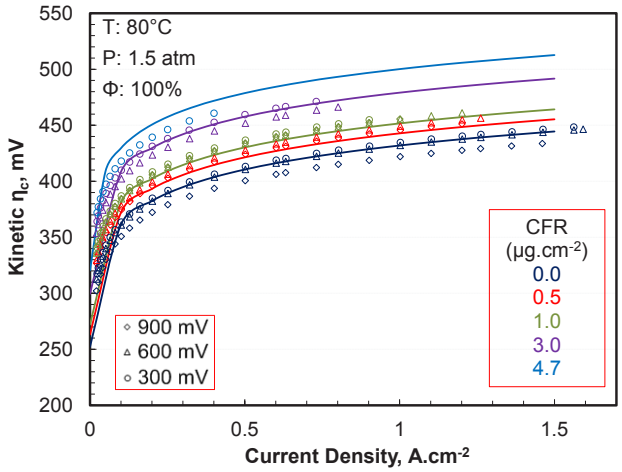


(a) Modeled ORR kinetic losses

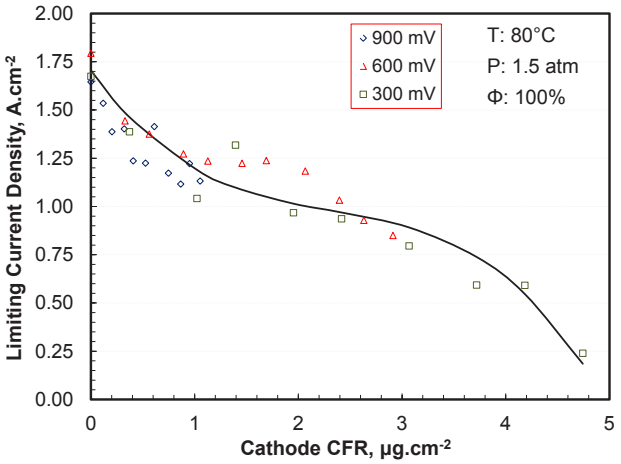


(b) Limiting current density correlation

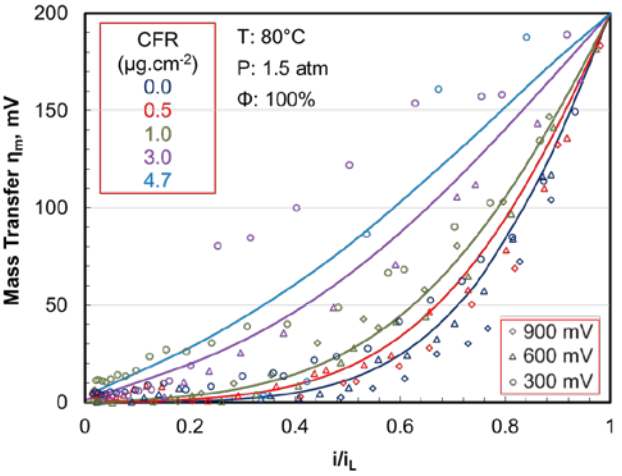


(c) Mass transfer correlation

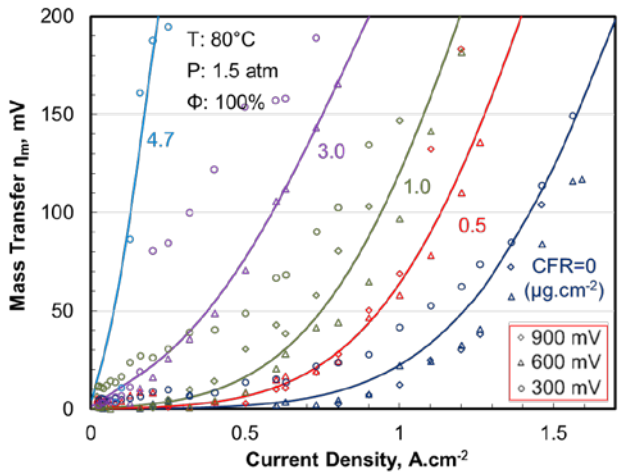


(d) Modeled mass transfer losses

**FIGURE 4.** Degradation model for NSTF catalyst based MEAs: (a) modeled ORR kinetic losses; (b) limiting current density correlation; (c) mass transfer correlation; (d) modeled mass transfer losses

lower cell voltages [6]. Although the measured fluoride release rates are an order-of-magnitude smaller than for Pt/C catalysts with state-of-the-art membranes [7], the resulting losses in cell voltage are much too high. Our next step is to quantify these losses on automotive cycles and develop strategies to mitigate them.

## CONCLUSIONS AND FUTURE DIRECTIONS

- Under optimum conditions (2.5-atm stack inlet pressure, 95°C coolant outlet temperature, and 86% cathode exit relative humidity) and using the BOC performance data, the projected platinum content and cost of an 80 kWe fuel cell system that meets the 1.45 kW/°C heat rejection constraint are 0.22 g/$kW_e$ and 53.8 \$/$kW_e$. The stack in this system has ternary PtCoMn/NSTF catalysts with Pt loading of 0.104 mg/$cm^2$ in the cathode and 0.05 mg/$cm^2$ in the anode.
- We have shown that GEN I d-PtNi/C has slight cost (\$/$kW_e$) and performance (g Pt/$kW_e$) advantages over Pt/C, especially at low pressures and temperatures. However, since the high surface area Pt/C is unstable under cyclic potentials, it is more appropriate to compare d-PtNi/C with a-Pt/C since the two catalysts have similar Pt particle diameters and should have similar stability. Our model indicates that d-PtNi/C can have 20–30% higher power density than a-Pt/C.
- We have confirmed that long potentiostatic hold is as a major degradation mechanism for the NSTF catalyst and that the irreversible performance losses are higher at lower cell voltages. Our next step is to quantify these losses on automotive cycles and develop strategies to mitigate the performance losses.

## FY 2015 PUBLICATIONS/PRESENTATIONS

**1.** R.K. Ahluwalia, X. Wang, W.B. Johnson, F. Berg, and D. Kadylak, "Performance of a Cross-Flow Humidifier with a High Flux Water Vapor Transport Membrane," J. Power Sources, Vol. 291, pp. 225–238, 2015.

**2.** D.D. Papadias, R.K. Ahluwalia, J.K. Thomson, H.M. Meyer III, M.P. Brady, H. Wang, R. Mukundan, and R. Borup, "Degradation of SS316L Bipolar Plates in Fuel Cell Environment: Corrosion Rate, Barrier Film Formation Kinetics and Contact Resistance," J. Power Sources, Vol. 273, pp. 1237–1249, 2015.

**3.** T. Hua, R.K. Ahluwalia, L. Eudy, G. Singer, B. Jermer, N. Asselin-Miller, S. Wessel, T. Patterson, and J. Marcinkoski, "Status of Hydrogen Fuel Cell Electric Buses Worldwide," Journal of Power Sources, Vol. 269, pp. 975–993, 2014.

**4.** R.K. Ahluwalia, X. Wang, "Performance of an Advanced Automotive MEA with Heat Rejection Constraint," IEA Annex 34 Meeting, Forschungszentrum Jülich, Jülich, Germany, June 24, 2015.

**5.** D. Myers, N. Kariuki, J. Hammons, R. Ahluwalia, X. Wang, J-K Peng, and D. Fongalland, "Dealloyed Pt-Ni Polymer Electrolyte Fuel Cell Cathodes: Effects of Catalyst-Ionomer Ink Composition on Structure and Performance," 227th ECS Meeting, Chicago, IL, May 24–28, 2015.

**6.** X. Wang, J-K Peng, R. Ahluwalia, D. Myers, and Z. Yang, "Mass Transfer Overpotentials in Dispersed Pt/C and De-Alloyed PtNi/C Polymer Electrolyte Fuel Cell Cathodes," 227th ECS Meeting, Chicago, IL, May 24–28, 2015.

**7.** R.K. Ahluwalia, X. Wang, T.Q. Hua, and D. Myers, "Fuel Cell Systems for Transportation: Recent Developments in U.S.A.," IEA Annex 26 Meeting, CEA, Grenoble, France, Dec. 3, 2014.

**8.** R.K. Ahluwalia, and N. Garland, "Report from the Annexes: Annex 26," IEA AFC ExCo 49th Meeting, CEA, Grenoble, France, Dec. 4–5, 2014.

## REFERENCES

**1.** Fuel cell technical team roadmap, http://energy.gov/sites/prod/files/2014/02/f8/fctt_roadmap_june2013.pdf, June 2013.

**2.** D. Myers, N. Kariuki, J. Hammons, R. Ahluwalia, X. Wang, J-K Peng, and D. Fongalland, "Dealloyed Pt-Ni polymer electrolyte fuel cell cathodes: Effects of catalyst-ionomer ink composition on structure and performance," 227th ECS Meeting, Chicago, IL, May 24–28, 2015.

**3.** A. Kongkanand and F. Wagner, "High activity de-alloyed catalyst," 2014 Hydrogen and Fuel Cells Program Review, FC087, June 16–20, 2014.

**4.** R.K. Ahluwalia, S. Arisetty, X. Wang, X. Wang, R. Subbaraman, S.C. Ball, S. DeCrane, and D. Myers, "Thermodynamics and kinetics of platinum dissolution from carbon-supported electrocatalysts in aqueous media under potentiostatic and potentiodynamic conditions," J. Electrochem. Soc. 160 (2013) F447–F455.

**5.** R.K. Ahluwalia, S. Arisetty, J-K Peng, R. Subbaraman, X. Wang, N. Kariuki, D.J. Myers, R. Mukundan, R. Borup, and O. Polevaya, "Dynamics of particle growth and electrochemical surface area loss due to platinum dissolution," J. Electrochem. Soc. 161 (2013) F291–F304.

**6.** A. Kongkanand, J. Zhang, Z. Liu, Y-H Lai, P. Sinha, E.L. Thompson, and R. Makharia, "Degradation of PEMFC observed on NSTF electrodes," J. Electrochem. Soc. 161 (2013) F291–F304.

**7.** A.J. Steinbach, K. Alade-Lambo, C. Hamilton, M.J. Kurkowski, R. Atanasoski, and M. Debe, "Reversible performance losses of PEM fuel cells," 238th ACS National Meeting and Exposition, Aug. 18, 2009.